Research Square

Preprints are preliminary reports that have not undergone peer review.
They should not be considered conclusive, used to inform clinical practice,
or referenced by the media as validated information.

The twisting direction of nAChR α7-ivermectin is opposite to that of the activated state

Yue Yang
Graduate School of Frontier Sciences, The University of Tokyo
Tatsuya Arai
Graduate School of Frontier Sciences, The University of Tokyo
DAISUKE SASAKI
Graduate School of Frontier Sciences, The University of Tokyo
Hidetoshi Inagaki
National Institute of Advanced Industrial Science and Technology (AIST)
Sumiko Ohashi
National Institute of Advanced Industrial Science and Technology (AIST)
Masahiro Kuramochi
Ibaraki University
Hiroshi Sekiguchi
Japan Synchrotron Radiation Research Institute
Kazuhiro Mio
National Institute of Advanced Industrial Science and Technology (AIST)
Tai Kubo
National Institute of Advanced Industrial Science and Technology (AIST)
Yuji Sasaki (ycsasaki@edu.k.u-tokyo.ac.jp)
Graduate School of Frontier Sciences, The University of Tokyo

Article

Keywords:

Posted Date: October 31st, 2022

DOI: https://doi.org/10.21203/rs.3.rs-2160678/v1

License: This work is licensed under a Creative Commons Attribution 4.0 International License.
Read Full License

Abstract

The alpha 7 nicotinic acetylcholine receptor (nAChR α7) is composed of five α7 subunits arranged symmetrically around a central pore. nAChR α7 is localized in the central nervous system and immune cells and could be a target for treating Alzheimer's disease and schizophrenia. Acetylcholine (ACh) is a ligand that opens the channel, although prolonged application results in a decrease in the response. Ivermectin (IVM) was reported as one of the positive allosteric modulators, since the binding of IVM to the channel enhances ACh-evoked alpha 7 currents. The molecular dynamics of the ligand-bound state of nAChR α7 have not been exhaustively studied.

We utilized a diffracted X-ray tracking method to monitor the twisting and tilting motion of nAChR α7 without a ligand, with ACh, with IVM, and with both ACh and IVM (ACh_IVM). The results showed that nAChR α7 twisted counterclockwise with the channel opening in the presence of ACh and clockwise without the channel opening in the presence of IVM. The mechanism of channel opening may be due to the twisting of the five α7 subunits together, where one or more of them are squeezed and move downward or upward.

Introduction

Ion channels are directly and/or indirectly involved in ion flux through the cell membrane, which leads to changes in cell excitability. Ion flux triggers subsequent signaling cascades in the cell and to the adjacent cells and contributes to homeostasis. The nicotinic acetylcholine receptor (nAChR) represents a ligand-gated ion channel (LGIC) that alters the ionic permeability of the membrane by binding acetylcholine or cholinergic ligands. Because of the high density of the receptor in the electroplax of *Torpedo* and the advancement of cDNA cloning technologies, biochemical and structure–function studies on the nAChR in the neuromuscular junction (NMJ) have accumulated[1,2] and have extended to the nAChRs in the central and peripheral nervous system[3] and in the immune system[4]. The nAChR in the NMJ consists of four kinds of homologous subunits assembled in a molar stoichiometry of a2, b, g (e), and d, and the a-subunit harbors the ACh-binding site[5–7]. The binding of agonistic ligands to nAChR induces ion flux through the channel formed by the pentameric subunits. Patch-clamp technology enabled insights into the electrophysiological behavior of a single channel of the nAChR[8], and together with kinetic studies, it was assumed that the nAChR has at least three different molecular dynamic substates in thermal reversible equilibrium: a basal or resting state (R), an active open channel state (A) and at least one desensitized state (D)[9]. Several approaches, such as X-ray crystallography, electron/cryo-electron microscopy[10,11], and in silico model analysis[12], can be used to visualize these states, which are possibly accompanied by conformational changes. However, there are currently no precise structural data providing details of the physiological transition in the receptor itself.

In a previous study, we applied the diffracted X-ray tracking (DXT) method to acetylcholine-binding protein (AChBP) and Torpedo nAChR. DXT is a method to track X-ray diffraction spots from gold nanocrystals labeled on an individual single protein in real time and real space[13]. We observed molecular

fluctuations of the proteins even without a ligand and observed the enhancement of tilting and twisting motions with the ligand[14].

In this study, we focused on neuronal nAChR α7 to observe molecular dynamic motions. The α7 receptor consists of homopentamer subunits arranged symmetrically around a central pore. It is highly expressed in both the hippocampus and cerebral cortex, suggesting the involvement of α7 in higher-order neural functions such as learning and memory[15]. Furthermore, significant correlations were shown between the impairment of α7 signaling and the cognitive deficits associated with Alzheimer's disease and schizophrenia[16–18]. For a therapeutic drug to treat Alzheimer's diseases and cognitive impairment associated with schizophrenia (CIAS), α7 signaling in the CNS would need to be augmented without affecting ACh binding to the allosteric site(s), which leads to favorable conformational change.

Ivermectin (IVM), a macrocyclic lactone, is an anthelminthic drug that targets glutamate-gated chloride channels (IC50 = ~ nM)[19,20]. It was also shown that IVM transiently potentiates α7 at micromolar concentrations when applied prior to ACh, while α7 shows no direct response to IVM[21]. Thus, IVM is classified as a type I positive allosteric modulator (PAM) for α7.

Here, to acquire more precise information on the molecular motions of nAChR in the three substates and their state-to-state transitions, we applied DXT to neuronal nAChR α7. nAChR α7 was labeled with gold nanocrystals via Met tags and fixed to the gold substrate by His tags. We define the patterns and directions of twisting (χ) and tilting (θ) motions of nAChR α7, as shown in Fig. 1a and 1b. We focused on the molecular dynamic motions of nAChR α7 with and without the ligand ACh and the type I PAM IVM (Fig. 1c).

Results And Discussion

Mean-square-displacement (MSD) analysis is often used in single-molecule tracking[22] to determine the degree of molecular motion and is also used in the analysis of DXT data[14,23,24]. Figure 2a shows the MSD curves derived from the angular-displacement distribution of the gold nanocrystals under four experimental conditions: ligand-free, in the presence of ACh, in the presence of IVM, and in the presence of both ACh and IVM (ACh_IVM). For the twisting (χ) direction, the degree of motion of nAChR α7 in order from largest to smallest was ligand-free, ACh, IVM and ACh_IVM. For the tilting (θ) direction, the degree of motion of nAChR α7 in order from largest to smallest was ligand-free, IVM, ACh and ACh_IVM. Both results show that bound ligands could restrict the freedom of nAChR α7 and decrease the twisting (χ) and tilting (θ) motions. To determine the complete 3D rotational motion of nAChR α7 more clearly, we combined the angular displacement distribution of gold nanocrystals in both the χ and θ directions as a normalized 2D motion map for each experimental condition (Fig. 2b and Supplementary Fig. S1 online). Due to the previous electrophysiological results, it is known that nAChR α7 can be activated by ACh to open the ion channel; however, the ion channel cannot open only in the presence of IVM. This led us to be more interested in the different dynamics of nAChR α7 caused by IVM and ACh. Therefore, we made 2D motion maps to show the differences between ACh_IVM and ACh or IVM conditions (Fig. 2c). These

results showed that the twisting (χ) motions of nAChR α7 were inhibited in the presence of IVM; however, the tilting ($\boldsymbol{\theta}$) motions did not change much. The twisting (χ) and tilting ($\boldsymbol{\theta}$) motions of nAChR α7 were both inhibited in the presence of ACh. Moreover, because the displacements shown in the 2D motion maps were absolute values and the changes of different conditions in the χ axis are more significant, we separated the overall motions according to the positive and negative directions in the χ axis, and the MSD curves (Fig. 2d, complete version in Supplementary Fig. S2 online) showed that the degree of motion of nAChR α7 ordered from largest to smallest was ACh (χ mode along negative direction: negative direction), ACh (χ mode along positive direction: positive direction), ACh_IVM (positive direction) and ACh_IVM (negative direction). This result indicates that the twisting (χ) motions observed in ACh and ACh_IVM conditions are opposite to one another, which demonstrates that IVM has the ability to twist nAChR α7 in the direction opposite to that of the ACh-activated state. Moreover, it is also known that the ion channel also opens when IVM is delivered before ACh, and the ACh-evoked currents will be enhanced due to the positive allosteric modulation of IVM[21], which may indicate that the mechanism of nAChR α7 channel opening is related to the different twisting (χ) directions and degrees of movements.

Similarly, the 2D motion maps showing the difference between the positive and negative directions in the χ axis (Fig. 3) were more intuitive for judging the trend of the motion caused by different conditions. However, before judging those trends, the meaning of the motion patterns of the positive and negative directions of the χ and $\boldsymbol{\theta}$ axes need to be understood. For the χ axis, motion in the positive direction means the sample twists clockwise, and motion in the negative direction means the sample twists counterclockwise (Fig. 1a). For the $\boldsymbol{\theta}$ axis, when the gold nanocrystal was labeled with the sample, as shown in Fig. 1b, because of Bragg's condition, the positive and negative directions of the $\boldsymbol{\theta}$ axis are meaningless, and only the magnitude is meaningful. According to the contour plots fitted by the 2D polynomial, we can see that in the ligand-free condition and the IVM condition, the 2D motion map can be divided into two areas, the area of positive motion in χ (red) and the area of negative motion in χ (blue). Those contour plots demonstrate that nAChR α7 showed positive twisting (χ) motions, while the tilting ($\boldsymbol{\theta}$) motions were stronger. However, in the presence of ACh, the 2D motion map could be divided into two areas but with inversive positions, meaning that nAChR α7 showed negative twisting (χ) motions and the tilting ($\boldsymbol{\theta}$) motions were stronger, opposite to the trends shown with IVM. In the presence of both ACh and IVM, the situation was more complex. The 2D motion map could be divided into four areas, which seem to have two mode motions in each plus and minus direction.

We also made pairs of difference 2D motion maps (Supplementary Fig. S3 online) under two different conditions, which seem to be meaningful. The results showed that compared to the ligand-free condition, the other three conditions all inhibited movement in both the χ and $\boldsymbol{\theta}$ directions, which agrees with the MSD results. We can see that the difference in motions between the ACh and IVM conditions is mainly in the χ direction; hence, we next focused on the motion patterns of each condition in the χ direction.

To analyze the twisting and tilting motion modes of the positive and negative directions of the χ axis, we used a normal Gaussian distribution to fit the histogram of the angular-displacement distribution of each condition (Fig. 4a; all conditions are shown in Supplementary Fig. S4 online). From that, we were most

interested in the difference between the ACh condition and IVM condition. Using the peak position, it can be roughly judged that in the presence of IVM, nAChR α7 is inclined to move in the positive direction (twist clockwise), and in the presence of ACh, nAChR α7 is inclined to move in the negative direction (twist counterclockwise). In the $\boldsymbol{\theta}$ direction (Supplementary Fig. S4b online), it was interesting that only the activated state of nAChR α7 tilted more when it twisted counterclockwise.

Therefore, to determine the specific motion patterns of each condition, we calculated the difference in the angular-displacement distribution in the positive and negative directions of the $\boldsymbol{\chi}$ axis for each condition and used the difference in the Gaussian fitting results in the positive and negative directions in Supplementary Fig. S4 as a simple fit. As shown in Fig. 4b, in the $\boldsymbol{\chi}$ direction, the ligand-free nAChR α7 showed predominantly clockwise twisting. In the presence of ACh, it twisted more in the counterclockwise direction with channel opening, and in the presence of IVM, nAChR α7 twisted more in the clockwise direction without channel opening. In the ACh_IVM condition, it twisted more in the counterclockwise direction, but the twisting was not as strong as in the ACh condition. It was demonstrated that IVM has the ability to twist nAChR α7 clockwise; however, the ion channel opens only when nAChR α7 twists counterclockwise (it does not open when nAChR is twisted clockwise. As shown in Fig. 4c, in the $\boldsymbol{\theta}$ direction, the ligand-free nAChR α7 tilted more while it twisted clockwise. In the presence of ACh, it tilted more when it twisted counterclockwise. In the presence of IVM, nAChR α7 tilted more when it twisted clockwise, similar to the ligand-free condition. In the ACh_IVM condition, when it twisted in the counterclockwise direction, it tilted less, which was different from the ACh condition.

We think the ion channel opening may follow Nigel's gating movement model[25], which states that when five α7 subunits are twisted together counterclockwise, one or more of them are squeezed and moved upward (Fig. 4d), resulting in a tendency to tilt more. In contrast, in the presence of IVM, when five α7 subunits are twisted together clockwise, one or more of the subunits are squeezed in the opposite direction and moved downward, also resulting in a tendency to twist more. Under the condition of ACh_IVM, which shows effects by both ACh and IVM, some α7 subunits may be squeezed and have a tendency to move upward and others move downward, resulting in less tilt; however, the ion channel still opens.

In addition, we also fitted the difference in the angular-displacement distribution in the positive and negative directions of the $\boldsymbol{\chi}$ axis for each condition directly by multiple normal Gaussian distributions (Supplementary Fig. S5 online), and the results were almost indistinguishable from those shown in Fig. 4. The only difference is in the $\boldsymbol{\chi}$ direction motion of nAChR α7 under ACh_IVM conditions, which showed that nAChR α7 had a tendency to twist clockwise, but since the area of this peak is very small, we still assume that this result is also due to the action of both ACh and IVM, that nAChR α7 twisted slightly clockwise and twisted strongly counterclockwise.

Method

Diffracted X-ray tracking We performed diffracted X-ray tracking in the Spring-8 BL40XU beamline by using white X-ray to monitor the twisting ($\boldsymbol{\chi}$) and tilting ($\boldsymbol{\theta}$) motions of nAChR α7 without a ligand, with ACh, with IVM, and with both ACh and IVM (ACh_IVM), with a time-resolution of 100 μs three times. nAChR α7 was labeled with gold nanocrystals (20–50 nm) via Met tags and fixed to the gold substrate by His tags. The X-ray diffraction spots in the Au(111) and Au(200) regions were recorded by an X-ray image intensifier and a CMOS camera.

Dxt Sample Preparation

The cDNA encoding rat alpha 7 nicotinic acetylcholine receptor (GeneBank S53987) was cloned by PCR using the newborn rat brain cDNA library as a template. We expressed the rat nAChR α7 (UniProt Q05941, Gly1-Ala480) in Xenopus oocytes by co-expressing the nAChR chaperones ric3 and NACHO, and the receptor was purified by the reported procedure[26]. To let nAChR α7 both connect to gold nanocrystals and gold substrates in the DXT experiment, we inserted a Met tag (MGGMGGMGGGS)[14] between the Pro17 and Leu18 in the N-terminal extracellular region, and a His tag between the Arg322 and Met323 in the cytoplasmic loop region.

In the DXT experiments, for gold-substrate preparation, we diluted 1 mg/ml of dithiobis (C2-NTA) to 0.8 mM with anhydrous ethanol and immersed the gold substrates into dithiobis solution for 24 hours and then in a 100 mM NiSO4 solution for 24 hours.

After the gold substrates were washed with phosphate-buffered saline (PBS, pH = 7.4), each substrate was dripped with 18 μl of nAChR α7 solution and incubated at 4°C for 6 hours. The proteins were fixed to the gold substrate by forming complexes of His residues and Ni-NTA. Each gold substrate was dripped with 60 μl of gold nanocrystal solution and incubated for 2 hours.

To prepare for the experiment, the unbound gold substrates were first washed with PBS. The gold substrate was dripped with 6 μl of PBS solution for the ligand-free condition. The gold substrate was dripped with 6 μl of 100 μM ACh in PBS solution for the ACh condition. The gold substrate was dripped with 6 μl of 30 μM IVM in PBS solution for the IVM condition. For the ACh_IVM condition, we preexposed nAChR α7 in 3 μl of 30 μM IVM solution for 1 minute, and then we added 3 μl of 100 μM ACh-PBS solution to the gold substrate.

Declarations

Ethics approval and consent to participate:

Not available.

Consent for publication:

Not available.

Availability of data and materials:

All data and materials described in this manuscript are included in this article.

Competing interests:

The authors declare that they have no conflict of interest.

Funding:

Funding information is not available.

Authors' contributions:

Y. Y, T. K. and Y.C.S. designed the experiments. K.M, T.K., H.I., and S.O. prepared the protein samples. T.A., D.S., M.K., H.S. and Y.C.S. performed the DXT experiments. Y.Y. and Y.C.S. analyzed the experimental data. Y.Y., T.K. and Y.C.S. wrote the manuscript.

Acknowledgements:

This work was supported by Ms. R. Kanou. This work was supported by JST CREST Grant Number JP18071859, Japan. DXT experiments were performed with the approval of the Japan Synchrotron Radiation Research Institute (Proposal Nos 2021B1393 and 2022A1337).

References

1. Weill, C. L., McNamee, M. G. & Karlin, A. Affinity-labeling of purified acetylcholine receptor from Torpedo californica. *Biochemical and biophysical research communications* **61**, 997-1003 (1974).
2. Noda, M. *et al.* Structural homology of Torpedo californica acetylcholine receptor subunits. *Nature* **302**, 528-532 (1983).
3. Albuquerque, E. X., Pereira, E. F., Alkondon, M. & Rogers, S. W. Mammalian nicotinic acetylcholine receptors: from structure to function. *Physiological reviews* (2009).
4. Fujii, T. *et al.* Physiological functions of the cholinergic system in immune cells. *Journal of pharmacological sciences* **134**, 1-21 (2017).
5. Karlin, A., Prives, J., Deal, W. & Winnik, M. Affinity labeling of the acetylcholine receptor in the electroplax. *Journal of Molecular Biology* **61**, 175-188 (1971).
6. Klymkowsky, M. W. & Stroud, R. M. Immunospecific identification and three-dimensional structure of a membrane-bound acetylcholine receptor from Torpedo californica. *Journal of molecular biology* **128**, 319-334 (1979).
7. Unwin, N. Nicotinic acetylcholine receptor and the structural basis of neuromuscular transmission: insights from Torpedo postsynaptic membranes. *Quarterly reviews of biophysics* **46**, 283-322 (2013).

8. Sakmann, B. & Neher, E. Patch clamp techniques for studying ionic channels in excitable membranes. *Annual review of physiology* **46**, 455-472 (1984).
9. Changeux, J.-P. & Edelstein, S. J. Allosteric receptors after 30 years. *Neuron* **21**, 959-980 (1998).
10. Nemecz, Á., Prevost, M. S., Menny, A. & Corringer, P.-J. Emerging molecular mechanisms of signal transduction in pentameric ligand-gated ion channels. *Neuron* **90**, 452-470 (2016).
11. Rahman, M. M. *et al.* Structure of the native muscle-type nicotinic receptor and inhibition by snake venom toxins. *Neuron* **106**, 952-962. e955 (2020).
12. Taly, A. *et al.* Normal mode analysis suggests a quaternary twist model for the nicotinic receptor gating mechanism. *Biophysical journal* **88**, 3954-3965 (2005).
13. Sasaki, Y. *et al.* Tracking of individual nanocrystals using diffracted x rays. *Physical Review E* **62**, 3843 (2000).
14. Sekiguchi, H. *et al.* Real time ligand-induced motion mappings of AChBP and nAChR using X-ray single molecule tracking. *Scientific reports* **4**, 1-9 (2014).
15. Dani, J. A. & Bertrand, D. Nicotinic acetylcholine receptors and nicotinic cholinergic mechanisms of the central nervous system. *Annu. Rev. Pharmacol. Toxicol.* **47**, 699-729 (2007).
16. Freedman, R., Hall, M., Adler, L. E. & Leonard, S. Evidence in postmortem brain tissue for decreased numbers of hippocampal nicotinic receptors in schizophrenia. *Biological psychiatry* **38**, 22-33 (1995).
17. Freedman, R. *et al.* Linkage of a neurophysiological deficit in schizophrenia to a chromosome 15 locus. *Proceedings of the National Academy of Sciences* **94**, 587-592 (1997).
18. Qi, X.-L., Nordberg, A., Xiu, J. & Guan, Z.-Z. The consequences of reducing expression of the α7 nicotinic receptor by RNA interference and of stimulating its activity with an α7 agonist in SH-SY5Y cells indicate that this receptor plays a neuroprotective role in connection with the pathogenesis of Alzheimer's disease. *Neurochemistry international* **51**, 377-383 (2007).
19. Cully, D. F. *et al.* Cloning of an avermectin-sensitive glutamate-gated chloride channel from Caenorhabditis elegans. *Nature* **371**, 707-711 (1994).
20. Lynagh, T. & Lynch, J. W. Ivermectin binding sites in human and invertebrate Cys-loop receptors. *Trends in pharmacological sciences* **33**, 432-441 (2012).
21. Krause, R. M. *et al.* Ivermectin: a positive allosteric effector of the α7 neuronal nicotinic acetylcholine receptor. *Molecular pharmacology* **53**, 283-294 (1998).
22. Saxton, M. J. & Jacobson, K. Single-particle tracking: applications to membrane dynamics. *Annual review of biophysics and biomolecular structure* **26**, 373-399 (1997).
23. Shimizu, H. *et al.* Global twisting motion of single molecular KcsA potassium channel upon gating. *Cell* **132**, 67-78 (2008).
24. Sekiguchi, H. *et al.* ATP dependent rotational motion of group II chaperonin observed by X-ray single molecule tracking. *PloS one* **8**, e64176 (2013).
25. Unwin, N. & Fujiyoshi, Y. Gating movement of acetylcholine receptor caught by plunge-freezing. *Journal of molecular biology* **422**, 617-634 (2012).

Figures

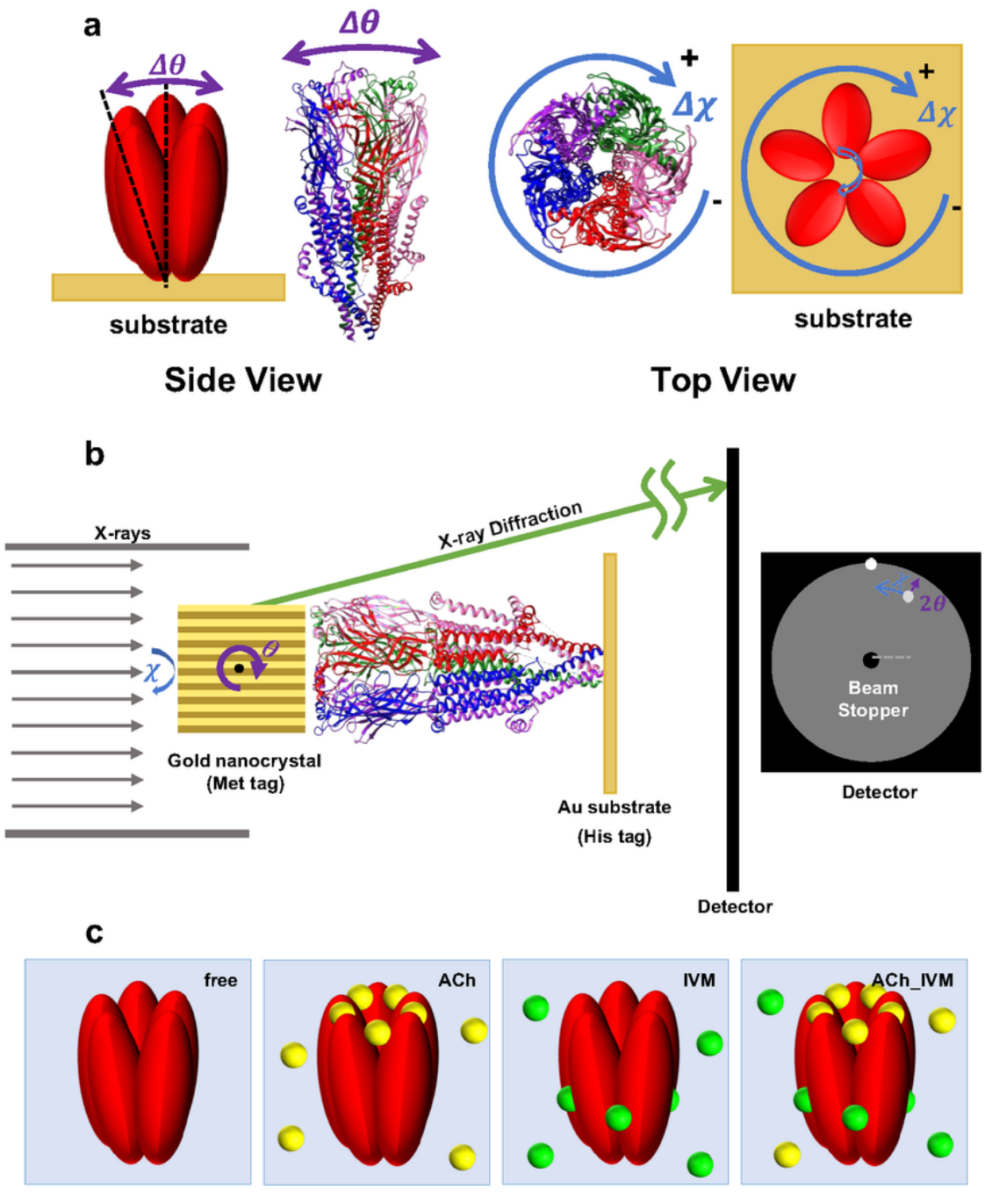


Fig. 1

Figure 1

Schematic diagram of experiments.

a Schematic diagram of nAChR α7 with tilting (θ) and twisting (χ) motions. nAChR α7 was labeled with gold nanocrystals via the Met tags and fixed to the gold substrate by His tags to measure the twisting (χ) and tilting (θ) motions, not the translation motion. **b**Schematic illustration of two modes of movement of nAChR α7 measured by the DXT method. By using the DXT method, the rotational motions of nAChR α7 could be monitored by tracking the X-ray diffraction spots from labeled gold nanocrystals. **c** Schematic diagram of four experimental conditions: without ligand, with ACh (yellow rounds), with IVM (green rounds), and with both ACh and IVM (ACh_IVM).

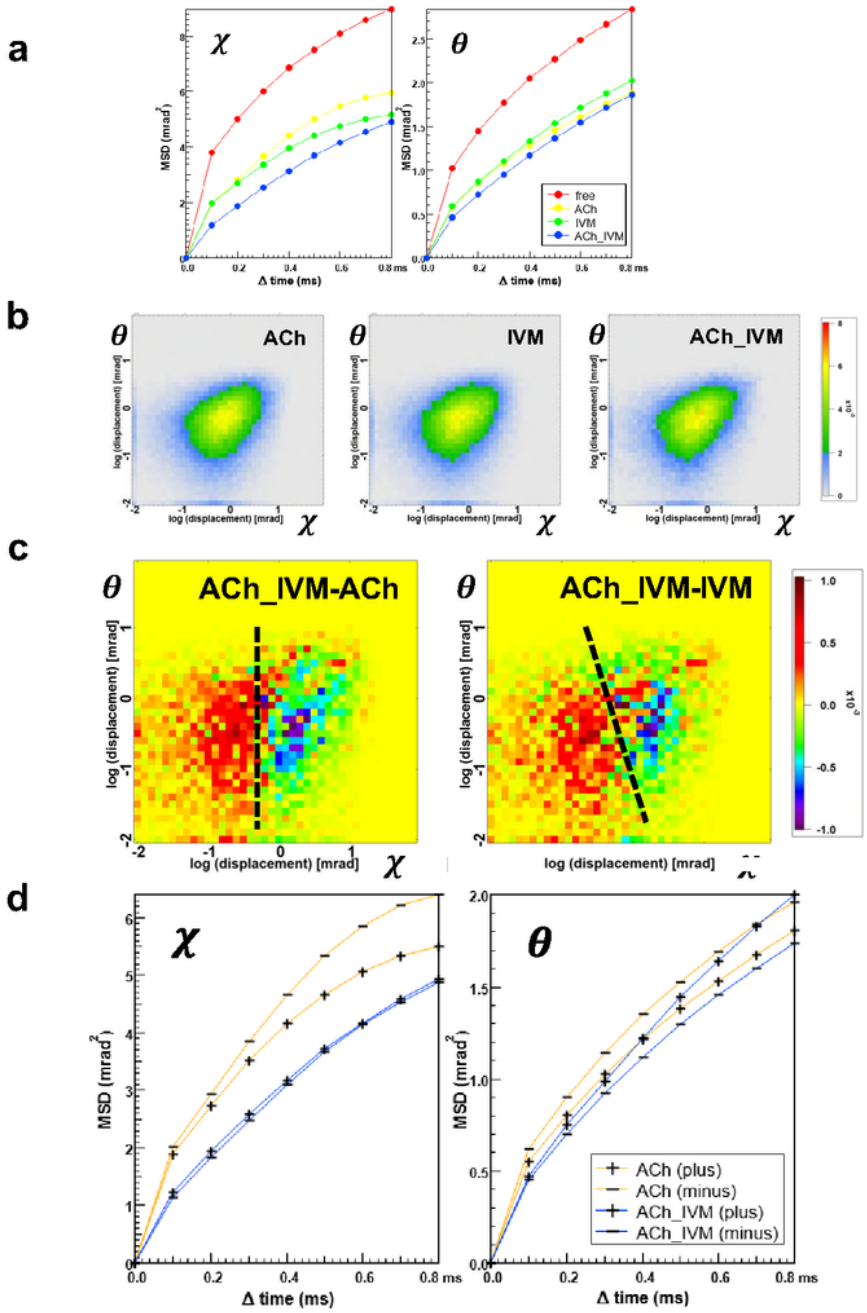


Fig. 2

Figure 2

DXT analyses.

a MSD curves of nAChR α7 in the twisting and tilting motion in the presence of nothing (red), ACh (yellow), IVM (green) or ACh_IVM (blue), showing the order of the degree of motion of nAChR α7 in 0.8 ms. **b** Normalized 2D motion maps of nAChR α7 in the presence of ACh, IVM, or ACh_IVM. All angular displacements are presented as absolute values. **c** Difference 2D motion maps between two conditions, showing that the twisting (χ) motions of nAChR α7 were inhibited in the presence of IVM and ACh. **d** MSD curves of twisting and tilting motions of nAChR α7 in the positive and negative directions of the χ axis in the presence of ACh or ACh_IVM, showing that IVM has the ability to twist nAChR α7 in the direction opposite to what it is when activated by ACh.

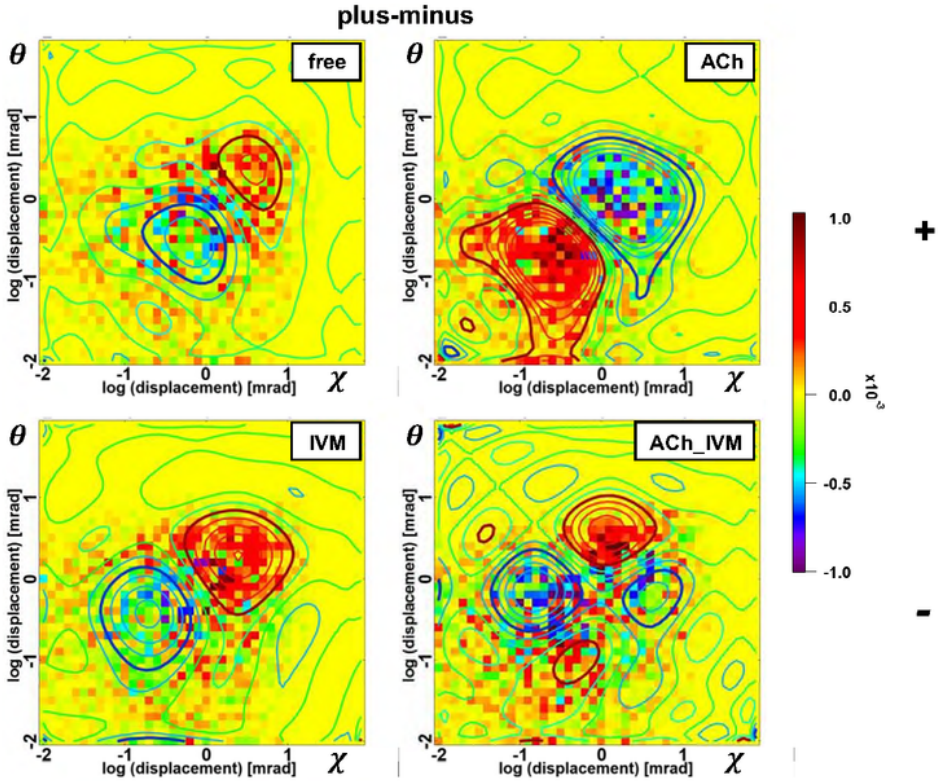


Fig. 3

Figure 3

Difference 2D motion contour maps.

The difference 2D motion contour maps between the positive and negative directions in the χ axis for all conditions. The red area is the area of positive χ motion, and the blue area is the area of negative χ motion.

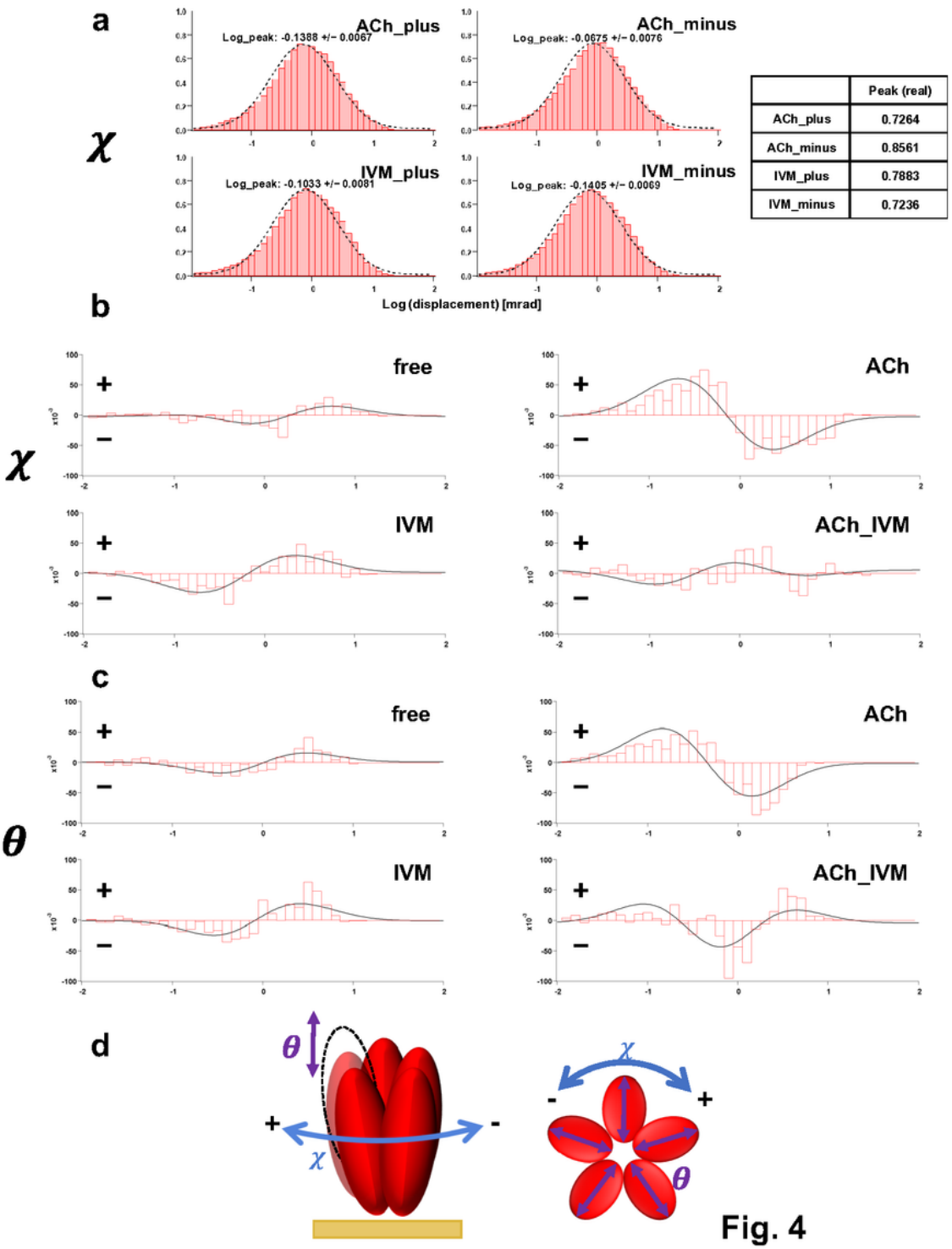


Figure 4

Difference angular displacement distributions.

aThe angular displacement distributions of twisting nAChR α7 in the positive and negative directions of the χ axis in ACh and IVM conditions (complete conditions shown in Supplementary Fig. S4 online). The difference angular displacement distributions in the positive and negative directions of twisting motion

(**b**) and tilting motion (**c**) were calculated for all conditions at this point. The fitting curves were made by the difference of the Gaussian fitting (black dashed line) results in the positive and negative directions in Supplementary Fig. S4. This result showed that the ion channel opens only when nAChR α7 twists counterclockwise. **d** Schematic diagram of the ion channel opening of nAChR α7. Five α7 subunits are twisted together, and one or more of them are squeezed and moved downward or upward.

Supplementary Files

This is a list of supplementary files associated with this preprint. Click to download.

- YYSupplementfigure.pdf